# Nanoscale

Check for updates

# Liposome purification from micromolar protein background using diffusiophoretic trapping

Pavlina Senikoglou, Corentin Cardot, Jonas N. Pedersen (ID) and Rodolphe Marie (ID) *

Colloid purification from liquid biopsies is a promising route for early diagnostics of complex diseases based on extracellular vesicle biomarkers. We have previously demonstrated that colloids, such as liposomes and exosomes, can be concentrated in a fluidic device by the combined effects of diffusiophoresis and diffusioosmosis induced by a salt gradient. The salt gradient imposed on an open channel causes an osmotic flow opposing the particle diffusiophoresis, which traps particles. Diffusioosmosis depends on the surface charge density of the device's inner walls. This is adjusted with a coating that also ensures that particle stiction is suppressed. When proteins are present at concentrations typically found in liquid biopsies, both aspects are challenged. Surface passivation by Pluronic polymers remediates these effects. We show that Pluronic effectively prevents adsorption of bovine and human serum albumin, as well as negatively charged liposomes, while maintaining a sufficiently high surface zeta potential to induce an osmotic flow that traps liposomes. Liposomes with a zeta potential of −30 mV and a diameter of 120 nm are captured from a dilute solution in the presence of bovine or human serum albumin at micromolar concentrations. The proteins are removed from the trap through diffusion while the liposomes remain trapped, and finally, we demonstrate how liposomes can effectively be purified from 10% plasma. These experiments bring diffusiophoretic trapping closer to practical applications in liquid biopsies.

## Introduction

Liquid biopsies contain proteins and colloids, *e.g.*, extracellular vesicles (EVs). EVs are lipid-based particles secreted by all cell types, composed of plasma membrane identical to those of their cells of origin. Smaller extracellular vesicles, called exosomes, have a diameter of 30–120 nm (ref. 1) and their concentration in plasma is in the range of $0.9–13.4 \times 10^8$ particles per mL.[2] Through endocytosis, important components from the cell's plasma membrane and its extracellular environment are internalized. Therefore, EVs carry important information about the cell of origin.[3] This has prompted the recent development of several methods for purifying EVs from liquid biopsies, such as blood, for diagnostic applications.[4]

While proteins and larger particles, *e.g.*, cells and cell debris, are effectively removed by centrifugation and filtration, colloidal particles with sizes and densities comparable to EVs present a greater challenge in EV purification from liquid biopsies. For instance, lipoproteins – complex particles that carry lipids and proteins – fall within the same size range as the smaller EVs. Ultra-centrifugation in density gradients can be used for EV purification, but it is time-consuming and may have a poor yield as it favors aggregation of EVs. This chal-

lenges further characterization of the isolated EVs, *e.g.*, determination of size and density.[5] These limitations have led to the development of alternative purification methods based on microfluidics, aiming for a more direct purification from original samples with minimal processing.[6]

In microfluidics, colloids are purified from a continuous stream of sample solution using field flow fractionation. As EVs are negatively charged, purification can be combined with size separation by electrophoresis if an external electric field is applied.[7] To circumvent the need for external fields, the spontaneous migration of charged particles in concentration gradients of electrolytes, so-called diffusiophoresis,[8] has attracted attention. Diffusiophoresis depends on both the particle's size and zeta potential, which makes it attractive for separating colloids by zeta potential within a well-defined size range. Diffusiophoresis generally occurs together with its counterpart diffusioosmosis, the transport of liquid induced by chemical gradients.[9] The combination of diffusiophoresis and diffusioosmosis has been applied to colloid separation in several geometries,[10] including closed channels,[11] dead-end channels,[12] Ψ-junctions with microgrooves,[13] H-junctions,[14] T-junctions,[15] and multiple non-collinear gradients.[16] In particular, a Ψ-junction flow-through device allowing surface chemistry-based continuous separation of colloids has been demonstrated.[17]

In a previous work, we used the combined action of diffusiophoresis and diffusioosmosis in an open channel to

*Department of Health Technology, Technical University of Denmark, Kongens Lyngby, Denmark. E-mail: rcwm@dtu.dk*

accumulate liposomes and exosomes from a dilute solution.[18] In this device, a salt gradient is imposed across an open channel, leading to a diffusioosmotic flow of solution with an effective velocity $u_{os}$. The Stokes' drag makes particles move along the flow (Fig. 1d). Due to diffusiophoresis, negatively charged liposomes move up the salt gradient with a velocity $u_{ph}$ (Fig. 1e). The diffusioosmotic flow counteracts the particle diffusiophoresis, leading to trapping. At the trapping position $x_0$, the particles' net velocity vanishes and they accumulate (Fig. 1f).

The zeta potential of the channel inner surface is a key element of the trapping as it drives the osmotic flow and prevents particles' stiction. For simple colloid samples, such as solutions containing only vesicles suspended in a buffer,[18–20] a phospholipid coating with a highly negative zeta potential (−20 to −30 mV) drives a sufficiently strong diffusioosmotic flow to support trapping and effective liposome repulsion.

This was successfully used to concentrate liposomes and exosomes diluted in phosphate buffered saline (PBS). However, blood components, *e.g.* proteins, are in micromolar concentrations, and EVs have complex surface compositions. So, applications of diffusioosmotic trapping to liquid biopsies require that the channel coating effectively suppresses protein and colloid adhesion, but also that it has a zeta potential that supports diffusioosmosis.

Pluronic is a family of biocompatible amphiphilic triblock polymers with a hydrophobic polypropylene oxide (PPO) block and two hydrophilic chains of polyethylene oxide (PEO). Pluronic molecules are categorized based on the hydrophilic–lipophilic ratio and the length of the PEO chain. Pluronic adopts a brush-like conformation on gold surfaces that reduces protein adhesion due to the extension of the hydrophilic PEO chains towards the solution.[21] Studies with Bovine Serum Albumin (BSA) show lower protein adhesion on hydro-
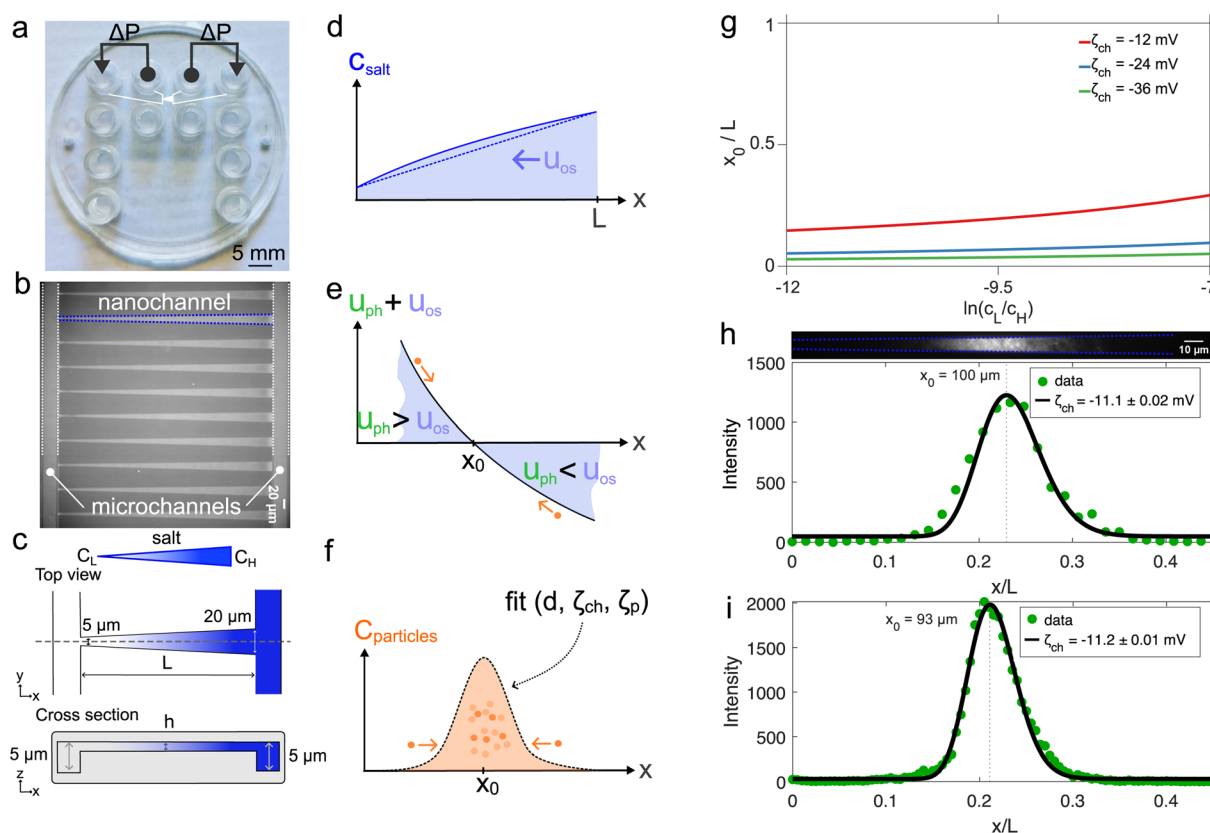


**Fig. 1** Principle of diffusiophoretic trapping. (a) Image of the injection molded chip. The arrows show the gas pressure connections used to drive the liquid inside the channels. (b) Bright field image of an array of nanochannels (blue outline) connected to two microchannels (white outline) at 20× magnification. (c) Top and cross sectional schematics of the funnel-shaped nanochannels. Channel length and height are $L = 440$ μm and $h = 295$ nm (Design 1). (d) A salt gradient is established across the nanochannels that induces a diffusioosmotic flow $u_{os}$. (e) The net particle velocity is the sum of the diffusioosmotic and the diffusiophoretic velocities, $u_{ph}(x) + u_{os}(x)$. The net velocity vanishes at the trapping position $x = x_0$. (f) Particles accumulate around the trapping position $x_0$, and the particle concentration profile $C(x)$ can be fitted with a model to characterize the particle diameter $d$, the zeta potential $\zeta_p$, and the channel wall zeta potential $\zeta_{ch}$. (g) Numerical simulations of the relative trapping position $x_0/L$ as a function of the salt gradient $\ln(C_L/C_H)$, for channel zeta potentials −12, 24 and 36 mV for Design 1. (h) Fluorescence image and corresponding intensity profile for trapped POPC : POPG : DiO 3 : 1 : 0.02 liposomes with $\zeta_p = -30$ mV and $d = 123$ nm (measured by ELS and DLS, respectively). (i) Intensity profile for trapped POPC : POPG : Biotin PE : DiO 3 : 1 : 0.02 : 0.02 liposomes with $\zeta_p = -29$ mV and $d = 119$ nm (measured by ELS and DLS, respectively) trapped in a nanochannel coated with Pluronic F-127 1% w/v. For (i) and (h), fits to the model for the concentration profile give the zeta potential of the coating.

phobic stainless steel with Pluronic F-68,[22,23] and on silicon wafers with Pluronic L-35, P-123, F-108.[24]

Pluronic F-127 is widely used due to its protein-repellent properties and its ability to form micelles in solution.[25] Therefore, while Pluronic F-127 is an attractive surface-passivation method for realizing a diffusiophoretic and diffusioosmotic trap capable of handling micromolar protein concentrations, its weak zeta potential may be a challenge for diffusiophoretic trapping because the induced diffusioosmotic flow may be too weak to counteract the particle diffusiophoresis.

Here, we demonstrate that Pluronic F-127 not only enables surface passivation but also supports trapping. We first measure the zeta potential of the cyclic olefin copolymer (COC) device surface coated with Pluronic. We then confirm that fluorescently labeled liposomes with a zeta potential in the range of −20 to −30 mV are trapped well within the nanochannel for a wide range of salt gradients. The Pluronic coating effectively prevents stiction, even for liposomes with a high degree of biotinylation, which typically adhere strongly to phospholipid-coated surfaces. Finally, we demonstrate how micromolar background proteins affect the zeta potential of the coating and find experimental conditions where liposomes reliably accumulate in the presence of a micromolar protein background. Next, the proteins are effectively removed from the nanochannel by diffusion, and the purified liposomes are upconcentrated in the nanochannel, which increases the fluorescence signal. Finally, we also show how an opposing protein gradient can be used to counter-balance the contribution of the plasma proteins to the diffusioosmotic flow, preventing liposomes from escaping the nanochannel, and maximizing the detected fluorescence signal.

## Results and discussion

### Pluronic coating for diffusiophoretic and diffusioosmotic trapping

Trapping is obtained by imposing a constant salt gradient across an open nanofluidic channel. Nanofluidic channels are fabricated as a single-use nanofluidic device produced by injection molding of COC. The final device is a disc (50 mm in diameter) with four reservoirs (two inlets, two outlets) shaped as LUER connectors. These allow loading of solutions and connection to a pressure control unit (Fig. 1a). Between each inlet and outlet runs a microchannel (50 μm wide, 5 μm deep). The microchannels are connected by an array of funnel-shaped nanochannels, 5 μm and 20 μm wide at the narrow and wide ends, respectively (Fig. 1b). The fluidic channels are sealed with a COC foil (175 μm thick) using UV-assisted thermal pressure bonding. In this work, we use two device designs with $L = 440$ μm (Design 1, identical to the work in ref. 18) and $L = 250$ μm (Design 2, see Methods and Fig. 1c).

A key step in preparing the device for diffusiophoretic trapping is the surface passivation of the micro- and nanochannels. An aqueous solution of the synthetic polymer Pluronic

F-127 at 1% w/v is used to passivate the surface.[26] We first check that the passivation of the surface with Pluronic leads to a negative osmotic flow of sufficient strength to balance diffusiophoresis and enable successful trapping of liposomes. To do this, we use a low ($C_L$) and high ($C_H$) salt concentration at the ends of the nanochannel to impose a strong salt gradient ($\ln(C_L/C_H) = -9.2$) and introduce negatively charged liposomes (zeta potential $\zeta_p = -30.1 \pm 1.4$ mV, and diameter $d = 122.8 \pm 0.6$ nm). A band of fluorescence in the channel indicates successful diffusiophoretic trapping within the Pluronic-coated device ($L = 440$ μm, Fig. 1h). We conclude that the surface is negatively charged and induces an osmotic flow (Fig. 1d) opposing the particle diffusiophoresis (Fig. 1e), resulting in particle accumulation (Fig. 1f). The particle concentration profile $C(x)$, proportional to the fluorescence intensity profile, has a maximum at $x_0$. At this trapping position, $u_{ph}(x_0) + u_{os}(x_0) = 0$ (Fig. 1e). The width of $C(x)$ is primarily determined by the Brownian motion of the particles, although dispersion resulting from a nonuniform flow velocity profile across the channel may also contribute (Fig. 1f).

Trapping occurs at $x_0/L \sim 0.25$ (Fig. 1h), while it occurs at $x_0/L \sim 0.04$ for the same liposomes and salt gradient using a highly negatively charged phospholipid coating.[18] A larger $x_0$ implies that the osmotic flow is weaker for the Pluronic coating (Fig. 1e), and consequently that the surface zeta potential $\zeta_{ch}$ is less negative (Fig. 1g).

In ref. 18 we derived a model for the particle concentration $C(x)$. Briefly, this model assumes an effective drift velocity depending on the zeta potential of the channel wall $\zeta_{ch}$ and a diffusiophoretic velocity scaling with $\ln(C_L/C_H)$. When $\zeta_{ch}$ is known from a flow calibration, $C(x)$ depends on the size and zeta potential of the particles. This simplistic model neglects several effects, e.g., the possible dispersion due to the flow velocity profile in the channel, the scaling of the DP velocity with the absolute salt concentration,[27] and the presence of other electrolytes in PBS solution besides sodium chloride, which could be accounted for ref. 11. Despite these limitations, the model describes trapping experiments with liposomes in the size range [70;160] nm and zeta potentials in the range of −[25;50] mV.[18] Here, we instead fit the zeta potential of the channel wall $\zeta_{ch}$, using the values of the particle diameter and zeta potential measured by Dynamic Light Scattering (DLS) and Electrophoretic Light Scattering (ELS), respectively, (diameter $d = 122.8 \pm 0.2$ nm and zeta potential $\zeta_p = -30 \pm 1.4$ mV) (Fig. 1h).

The fitted value of the wall zeta potential for the Pluronic coating on COC is $\zeta_{ch} = -11.10 \pm 0.02$ mV, consistent with the mean of four adjacent nanochannels −11.17 ± 0.05 mV (Fig. S1) and previous studies.[28] In solution, Pluronic micelles loaded with curcumin show a weak zeta potential (Pluronic P-123 with $\zeta_p = -7.37$ mV and Pluronic F-127 with $\zeta_p = -13.93 \pm 1.07$ mV.[28] Moreover, when Pluronic is used as a coating, it tends to reflect the properties of the material underneath. For example,[29] silver nanoprisms with highly negative zeta potential coated with 1.25% (w/v) Pluronic solution exhibit a −10 mV zeta potential due to screening.

Next, we investigate whether the Pluronic coating also suppresses stiction of colloids with more complex surfaces. To test this, we repeat the experiment with biotinylated liposomes (Fig. 1i). The diffusiophoretic trapping of biotinylated liposomes typically fails using a phospholipid coating as they are prone to stiction due to the hydrophobicity of the biotin moieties (Fig. S2). In contrast, stiction is suppressed by a Pluronic coating, and biotinylated liposomes are successfully trapped at $x_0/L \sim 0.2$. A fit of the concentration profile with the zeta potential and size of the liposomes measured with ELS and DLS, respectively ($\zeta_p = -29.8 \pm 2.9$ mV and $d = 119 \pm 1$ nm) gives a zeta potential of the channel of $\zeta_{ch} = -11.80 \pm 0.01$ mV, consistent with the mean of four adjacent nanochannels $-11.70 \pm 0.21$ mV (Fig. S1f–j), and close to the values obtained for the non-biotinylated liposomes ($\zeta_{ch} = -11.17 \pm 0.05$ mV, Fig. S1e).

## Liposome purification from solutions with BSA and HSA

After demonstrating that the Pluronic coating supports diffusioosmosis and trapping, we investigate the effect of the protein background on the trapping of liposomes, and demonstrate how proteins affect the channel walls. This is done in three steps.

First, a $L = 440$ μm nanochannel device (Design 1) is coated with Pluronic (1% w/v) to trap well-characterized DiO-labeled liposomes in a strong salt gradient ($\ln(C_L/C_H) = -9.2$) without proteins. After one minute of constant accumulation, liposomes are removed from the microchannels and a fixed amount of particles is trapped. A plot of the fluorescence distribution in the nanochannels (blue curve in Fig. 2a) and a fit to $C(x)$ with the zeta potential of the channel wall as the only fitting parameter shows that $\zeta_{ch} = -11.8$ mV (Fig. S3a).

Next, the liposomes are removed from the nanochannel with a pressure-driven flow. A new sample solution containing both liposomes (20.7 nM of particles) and BSA (2 μM) is introduced from the low salinity microchannel using the same salt gradient (−9.2).

A linear increase of the fluorescence signal in the channel indicates that liposomes accumulate continuously. This is also observed in the absence of proteins when a constant concentration of particles is present in the microchannel (Fig. 2b). The trapping position $x_0$ initially increases over time (Fig. 2c), and the particle distribution becomes wider (Fig. 2d) as the trapping position moves further into the nanochannel.

Finally, we assess whether the protein background can effectively be removed from the trap, and if BSA has irreversibly altered the zeta potential of the channel walls. For this purpose, the BSA solution containing liposomes is flushed out of the nanochannel by an applied pressure. A new liposome solution without BSA is introduced to the microchannel at the same salt gradient (−9.2). Liposomes are trapped at a position similar to the trapping position obtained before the device was exposed to BSA (Fig. 2a, yellow curve). A fit of the new fluorescence intensity profile gives approximately 1 mV difference in $\zeta_{ch}$ (Fig. S3b) compared to the $\zeta_{ch}$ measured before BSA was introduced. This shows that the effect of BSA adsorption on the nanochannel walls – if present – is minimal and reversible.

We also notice that the integrated intensity of the fluorescence band is proportional to the total number of particles in the trap, and that intensity profiles shown for different times of an experiment can be compared as they all are recorded with the same illumination and exposure time. So, conditions leading to trapping at smaller $x_0/L$ yield a narrower distribution and a higher peak intensity for a constant number of trapped particles.

In Fig. 2c, the initial change of trapping position before saturation is likely due to the build-up of a protein gradient in the nanochannel, which may influence both the osmotic flow rate and the diffusiophoretic velocity of the particles, as neutral and electrolyte solutions have been shown to induce diffusioosmosis.[30,31] The 2 μM BSA solution at the low salinity microchannel diffuses into the nanochannel, and a gradient establishes on a characteristic time scale $\tau \simeq \frac{L^2}{\pi^2 D} \sim 5.6$ minutes based on the albumin diffusion coefficient $D = 58$ μm$^2$ s$^{-1}$. This characteristic time scale assumes no convection along the nanochannel, which is not the case in our experiment due to the presence of the opposing osmotic fluid flow. We thus expect the gradient to be establish slower than the characteristic time scale, but the characteristic time scale for setting up the gradient is short enough compared to the duration of the experiment that one can reasonably assume that the protein gradient is stable after 25 minutes. Assuming a linear protein concentration gradient between the two microchannels, the protein concentration at the trapping position is estimated to be 75% of the protein concentration in the microchannel, i.e., 1.5 μM. This follows from assuming that the protein concentration as a position $x$ along the nanochannel is $C(x) = C_{wide} - \frac{x}{L}(C_{wide} - C_{narrow})$, and for $x_0 \simeq L/4$ and $C_0$ the introduced protein concentration at the microchannel, $C(x_0) = 0.75 \times C_0$.

BSA is used in research as a model for Human Serum Albumin (HSA) present in blood. BSA and HSA are homologous proteins, but structural differences, such as a higher fraction of α-helices in HSA, make HSA more hydrophobic than BSA.[32] We repeat the experiment with 8 μM HSA. First, we introduce a solution with liposomes and HSA using a strong salt gradient (−9.2). Liposomes initially accumulate in the trap at $x_0/L \sim 0.25$ (Fig. 2e, '1 min' curve). For the next 30 minutes, the fluorescence signal in the trap increases linearly indicating a steady accumulation of particles (Fig. 2f). The trapping position $x_0$ moves further into the channel and the full width at half maximum (FWHM) of the distribution increases, similar to observations for 2 μM BSA (Fig. 2a). Both values reach steady state levels (Fig. 2g and h). Next, the sample solution in the microchannel is exchanged with a clean low salinity buffer. Liposomes stay trapped but their trapping position moves towards the entrance of the nanochannel, indicating that the HSA is removed from the nanochannel by diffusion (Fig. 2e, yellow curve). Finally, the liposomes are trapped at $x_0/L \sim 0.2$. A fit of the liposome fluorescence intensity profiles after HSA removal (Fig. S4) results in the same channel wall zeta potential as observed in absence of proteins. This confirms the successful removal of HSA in the micromolar range from the colloid sample in a Pluronic coated nanochannel.
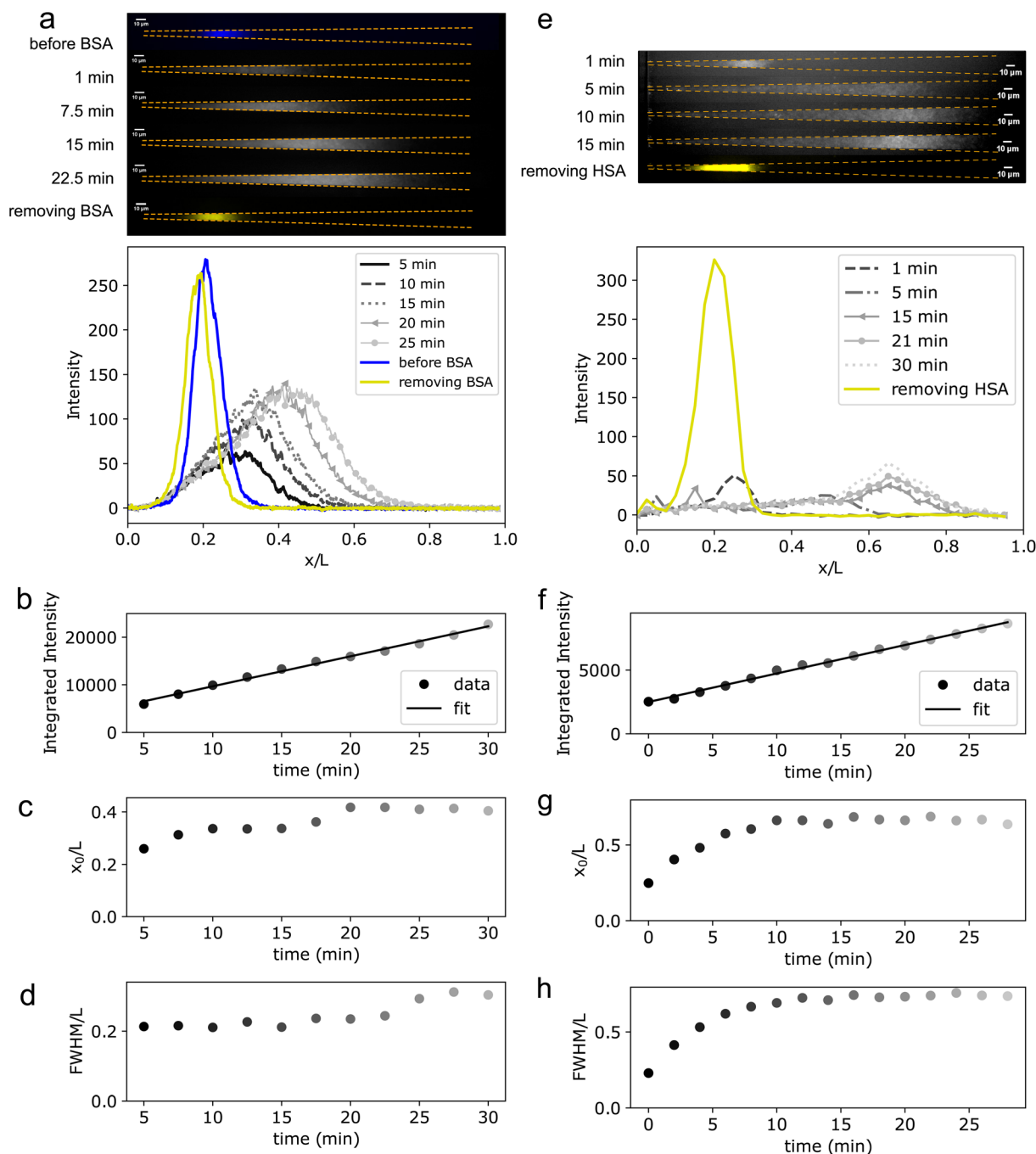
**Fig. 2** Trapping of liposomes (POPC : POPG : DiO 3 : 1) in BSA and HSA backgrounds. (a) Evolution of trapping position (gray) with continuous trapping of liposomes in a 2 μM BSA solution. The liposome distribution before (blue) and after (yellow) removal of the protein is shown. (b) Linear increase in total fluorescence intensity from the liposome distribution in a 2 μM BSA solution. (c) Trapping position $x_0$ versus time after introduction of BSA, and (d) FWHM values obtained from fits to the model for the intensity profile. (e) Recording of the liposome intensity profiles during introduction of a 8 μM HSA solution spiked with liposomes for 30 minutes (gray curves), and after HSA has been removed (yellow curve). (f) The integrated liposome intensity, (g) the trapping position $x_0$, and (h) the FWHM of the profile width. All experiments are performed with device Design 1 ($L$ = 440 μm).

## Liposome purification from plasma

EVs purification from plasma by diffusiophoretic trapping poses a number of challenges. First, the relatively low abundance of EVs compared to proteins is a major challenge. Exosomes in

healthy human plasma are present at $10^8$ to $10^{10}$ particles per mL concentration,[33] while HSA is found at concentrations seven orders of magnitude higher (35–50 g $L^{-1}$, *i.e.*, in the $10^{17}$ particles per mL range). This we address by using the superior anti-stiction properties of the Pluronic coating.

However, the ionic strength of plasma is also a concern for diffusiophoretic trapping. Human plasma has an ionic strength that is similar to a 1× PBS buffer solution.[34] To create a sufficient salt gradient against a high salt solution (10× PBS), we must dilute the sample, which also means diluting the EV concentration. The osmotic flow rate and the osmotic flow velocity scale with the length of the nanochannel as $v_{os} \sim \ln(C_L/C_H)/L$. To minimize sample dilution, we use a shorter trap. Here, we note that because of the funnel-shaped nanochannel, the higher the gradient, the higher the detected fluorescence signal. Thus, to minimize sample dilution, we use device Design 2 ($L = 250$ μm), which generates approximately twice the diffusiophoresis strength compared to Design 1 for the same sample dilution (1 : 10).

In the following experiment, we first trap fluorescent liposomes (POPC : POPG 3 : 1, $d = 123$ nm and $\zeta_p = -30$ mV) suspended in a $10^{-3} \times$ PBS solution in the absence of proteins (Fig. 3a, 'liposomes'). For the strong salt gradient ($\ln(C_L/C_H) = -9.2$), the trapping position is at $x_0/L \sim 0.25$ (Fig. 3b, dotted curve). Keeping the liposomes in the trap, diluted plasma (1 : 10) is introduced in the low salt microchannel, changing the salt gradient value to $\ln(C_L/C_H) = -4.6$. As anticipated, the liposome trapping position moves further into the nanochannel and the distribution of trapped particles becomes wider (Fig. 3a, 'liposomes in plasma', and Fig. 3b, solid curve). Finally, a protein-free $10^{-3} \times$ PBS solution is introduced in the

microchannel, and liposomes are removed from the nanochannel to show that there is no particle stiction on the nanochannel walls (Fig. 3a, 'washing', and Fig. 3b, dashed curve). This highlights that the Pluronic coating prevents non-specific interactions of proteins and liposomes with the nanochannel walls at high protein concentrations (~100 μM for 10% plasma).

In the initial experiment with plasma depicted in Fig. 3, the trapping position in the presence of plasma is much further inside the nanochannel. Before further investigations, we confirm that trapping liposomes in both designs is similar. To this end, we trap liposomes and measure the wall zeta potential in five individual experiments for each device design, and get that $\zeta_{ch} = -11.5 \pm 0.1$ mV for Design 1, and $\zeta_{ch} = -10.24 \pm 0.09$ mV for Design 2, indicating a design-specific offset (Fig. S5). We attribute this offset to a design-specific residual flow, *i.e.*, a flow induced in the nanochannels by the pressure driven flow in the microchannels. The residual flow rate can be determined from a calibration of the osmotic flow rate.[18] The resulting residual flow rate of $-28$ fL min$^{-1}$ (Fig. S6) for the $L = 440$ μm chip (Design 1) is in good agreement with previous measurements for the same device.[18] In contrast, we expect that the residual flow plays a larger role for the design with the shorter nanochannel ($L = 250$ μm) as it has a lower hydrodynamic resistance. However, for equal salt gradients, a shorter nanochannel should also give a larger diffusioosmotic flow due to the lower hydrodynamic resistance. We conclude that although the residual flow in the shorter nanochannel device Design 2 is stronger compared to Design 1, it is still negligible compared to the osmotic flow, and results in similar trapping. This is confirmed by the fact that trapping liposomes in the presence of 1 μM BSA in Design 2 matches the results obtained with Design 1 (Fig. S7).

We thus conclude that the main reason for the observed change in trapping position is the presence of a strong protein gradient induced by the introduction of plasma. We suspect this causes an additional contribution to the overall diffusioosmosis and diffusiophoresis, leading to a shift of the trapping position. It is a definite drawback for particle trapping since particles could escape when the particle distribution overlaps with the channel end at $x = L$. To minimize this, we balance the protein gradient induced by the diluted plasma (1 : 10 dilution) on the low salinity microchannel by adding BSA at 100 μM at the high salinity microchannel. We first trap liposomes in the absence of proteins at a strong gradient ($\ln(C_L/C_H) = -9.2$) (Fig. 4a). The fluorescence intensity profile shows a trapping position $x_0/L \sim 0.25$ (Fig. 4b). Next, the same liposomes are trapped from a 10% plasma solution while BSA is added to the high salinity channel. Fluorescence images after 15 and 30 min of accumulation (Fig. 4a) show a trapping position shifted, but close to, $x_0/L \sim 0.25$ (Fig. 4c and d). The lowered strength of the salinity gradient ($\ln(C_L/C_H) = -4.6$) when diluted plasma is used largely explains the shift of trapping position. So, the osmotic flow contribution induced by the protein gradient can largely be counterbalanced. Hence, the trapped liposomes do not escape, which improves the trap-
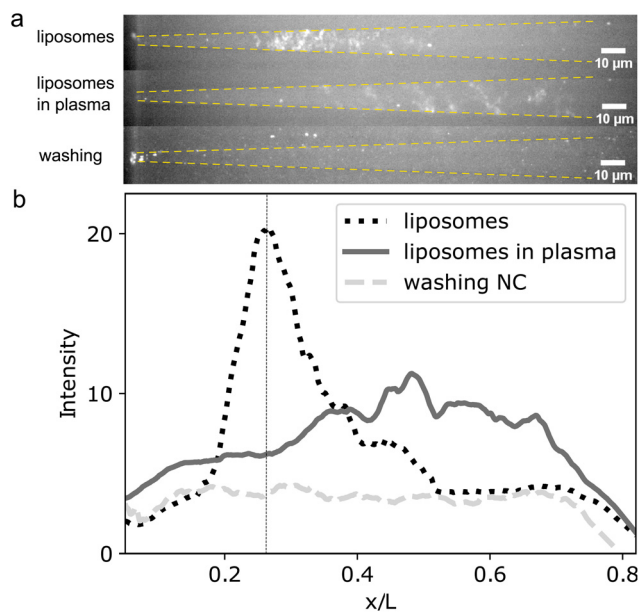


**Fig. 3** Liposomes (POPC : POPG : DiO 3 : 1) in 10% plasma. (a) Fluorescence images of the liposomes in a nanochannel when liposomes are trapped alone, in the presence of plasma, and after washing. (b) Fluorescence intensity profiles of the liposome signal. The dotted line shows liposomes trapped in a Pluronic 1% coated nanochannel (Design 2, $L = 250$ μm) using a strong salt gradient ($-9.2$). The gray solid line represents liposomes while plasma is introduced ($\ln(C_L/C_H) = -4.6$) for 30 minutes. The dashed line shows the fluorescence intensity after the liposomes are flushed out of the nanochannel.
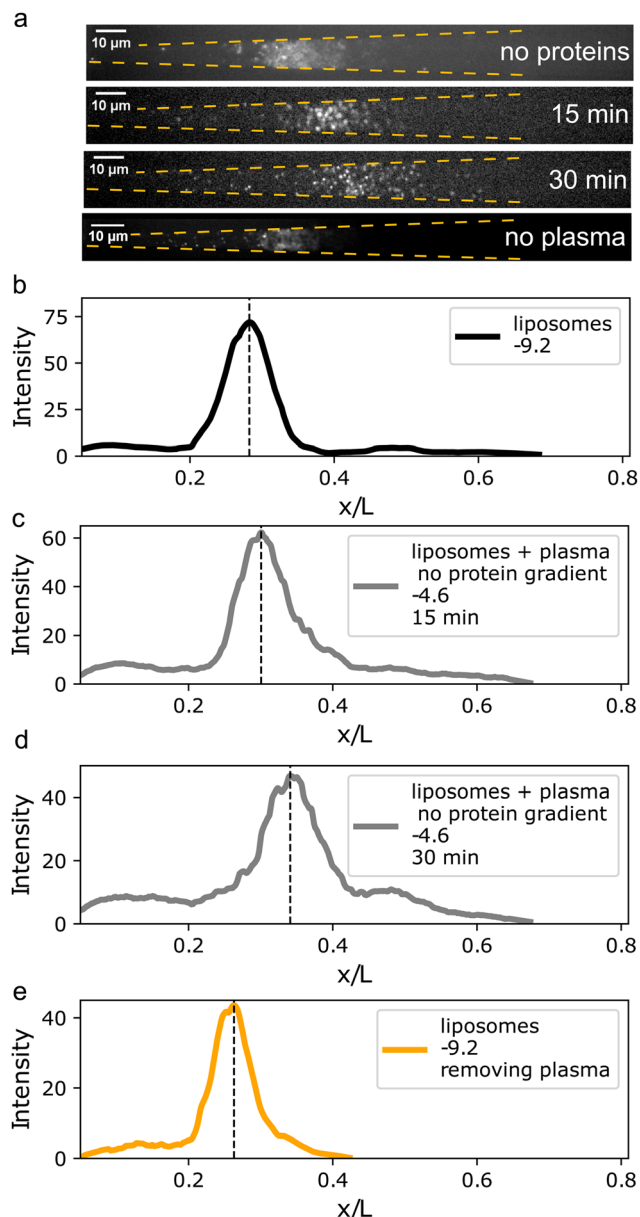
**Fig. 4** Liposomes (POPC : POPG : DiO 3 : 1) in 10% plasma with balanced protein concentration. (a) Fluorescence images corresponding to plots (b–e) showing liposomes accumulated from plasma after 15 min, 30 min, after removal of the proteins, and in the absence of proteins. (b and c) Liposomes trapped in a strong gradient ($\ln(C_L/C_H)$ = −9.2). Plasma (1 : 10 dilution) and BSA (100 μM) are introduced from the low and high salinity microchannel, respectively. The fluorescence intensity profile after (b) 15 and (c) 30 minutes. (d) Same liposomes after protein is removed from the nanochannel. (e) Liposomes accumulated in the same device in the absence of proteins. Nanochannel length is $L$ = 250 μm (Design 2) in all measurements.

ping efficiency. Finally, as the last step of the experiment, protein-free solutions are introduced to the microchannels (Fig. 4a and e), allowing proteins to diffuse out of the nanochannel. At this stage, the used salt concentrations lead to a strong salt gradient ($\ln(C_L/C_H)$ = −9.2), so the trapping position moves closer to the narrow end of the nanochannel. The lipo-

somes are thus not only purified from the proteins but also further concentrated by the combined effect of the nanochannels' funnel shape and the diffusiophoretic action. Due to the reduced width of the nanochannel and the fact that particle distributions are narrower for $x_0/L \to 0$, the fluorescence signal from the accumulated liposomes is maximized when $x_0/L$ is minimized (Fig. 4e). Fitting of the liposome distribution before introduction of the plasma sample and after removal of the proteins shows successful purification from the proteins, while the channel zeta potential remains unchanged (Fig. S8).

Finally, we note that during the experiment the maximum ionic strength experienced by the particles is for $x_0/L \sim 0.5$ in a gradient corresponding to $\ln(C_L/C_H)$ = −4.6. Here we estimate the ionic strength to be 5× PBS, approximating the salt concentration with a linear function.[35] The stability of the liposomes at such high ionic strength may be a concern. However, at this stage of the experiment, liposomes are in the presence of serum proteins. Serum proteins, such as albumin, form a protein corona[36] and may help prevent particle aggregation and fusion,[37] which is otherwise favored by the high ionic strength.

## Conclusions

We have demonstrated that diffusiophoretic trapping in open nanochannels can be realized after passivation of the channel walls with Pluronic. The polymer suppresses both colloid and protein adsorption. After passivation with Pluronic, the zeta potential of the channel wall is approximately −11 mV. The zeta potential of the channel wall and the imposed salt gradient across the channel induce an osmotic flow that balances the diffusiophoresis of negatively charged liposomes. Consequently, particles accumulate at the trapping position $x_0/L \sim 0.25$.

When colloids are initially suspended in a protein solution, *e.g.*, diluted plasma, the osmotic flow induced by the protein gradient may shift the trapping position towards the end of the channel ($x_0/L \sim 1$). This could cause particles to escape the trap, significantly decreasing the particle concentration. This can be alleviated by an opposing gradient of 100 μM BSA in the microchannel with high salt. Under such balanced conditions, the ionic strength gradient alone drives the diffusioosmotic flow, and liposomes suspended in 10% plasma accumulate in the trap. When the plasma and BSA solutions are replaced by buffer solutions in the microchannels, the proteins diffuse out of the nanochannel. This separates the liposomes from the proteins, and the concentrated colloids are purified in the trap. Our results thus provide a practical strategy for applying diffusiophoretic trapping to the characterization of particles isolated from serum.

## Materials and methods

### Liposome synthesis and solutions

In this experiment, 1-palmitoyl-2-oleoyl-*sn-glycero*-3-phosphocholine (POPC, Avanti, CAS Number: 26853-31-6, Catalog nr:

850457P), 1-palmitoyl-2-oleoyl-*sn*-glycero-3-[phospho-*rac*-(1-glycerol)] (sodium salt) (POPG, Avanti, CAS Number: 268550-95-4, Catalog nr: 840457P), and 1,2-dipalmitoyl-*sn*-glycero-3-phosphoethanolamine-*N*-(biotinyl) (sodium salt) (Biotinyl PE, Avanti, CAS Number: 384835-54-5, Catalog nr: 870285P) are used to fabricate liposomes. The liposomes are labeled with a lipophilic fluorescent stain, DiO (DiOC18(3) (3,3′-dioctadecyloxacarbocyanine Perchlorate)). Each lipid powder is placed in the desiccator to reach room temperature slowly and avoid denaturation of the lipids due to moisture. Each lipid powder is weighted in glass vials and then dissolved in *tert*-butanol 9 : 1. One final solution is prepared by mixing POPC and POPG lipid solutions, and finally adding DiO. For biotinylated liposomes Biotinyl PE is also added. The solution is snap-frozen with liquid nitrogen and undergoes freeze-drying overnight. Then, the product powder is hydrated with phosphate-buffered saline (1× PBS) to form a polydisperse liposome solution. The solution is heated at 50 °C and is vortexed every 15 min for 1 h. The liposomes are extruded through polycarbonate filter membranes of variable porosity depending on the desirable end diameter (here the filter is 100 nm). The liposomes are passed through the mini-extruder 21 times to produce a monodisperse solution. Liposomes stock solution was at a concentration of $3.12 \times 10^{10}$ particles per L estimated from the concentration of lipids (5 μmol mg$^{-1}$). Liposomes were further diluted in dilutions of 1× PBS to reach the desired salt concentration. Protein powders BSA (Thermofisher, protease free, CAS: 9048-46-8, Catalog nr: 268130100) and HSA (Sigma Aldrich, lyophilized powder ≥ 96%, CAS: 70024-90-7, Catalog nr: A1653) were dissolved and diluted in 1× PBS at 500 mg mL$^{-1}$ then stored at −20 °C. Before use, the BSA or HSA stock was further diluted to reach the desired salt concentration. Blood from donors at Rigshospitalet was collected in the morning of the experiment from healthy, same-blood-group donors (routinely screened for HIV, Hepatitis B and C, hemoglobin, and periodically iron levels). The blood remained unclotted with EDTA and was aliquoted in 0.5 mL vials that is pooled together in Protein LoBind Eppendorf vials. The blood was centrifuged at low speed for a short time (Centrifuge 5430, FA 45-30-11 rotor with 8.2 cm radius). In detail, to remove the cells the sample was centrifuged at 400*g* for 5 minutes to remove platelets in blood, and then at 2000*g* for 15 minutes to remove remaining cell debris. Finally, the plasma is passed through two membrane filters (0.45 μm, 0.22 μm pore filter size, Thermofisher Catalog number CH4513-CA, Thermofisher Catalog number CH2225-PES). Plasma and 1× PBS have a similar ionic strength,[38] thus the plasma is diluted appropriately to resemble the desired salt concentration.

### Dynamic light scattering and electrophoretic light scattering

The liposomes' zeta potential and diameter are measured by ELS and DLS respectively (Zetasizer Nano, Malvern) using a DTS1070 cuvette for the zeta potential and disposable cuvettes for diameter. The ionic concentration of the buffer used to extract zeta potential with ELS is important as a high salt solution could in principle compress the particle's double layer and screen its surface charge. Thus, the buffer used in all DLS/ELS measurements is 1× PBS. Finally, the cleanness of the cuvettes can be a challenge with DLS as dust impurities scatter light strongly. Hence, the cuvettes use here are first rinsed with pure ethanol to enhance wettability, and then with the buffer to be used (1× PBS) before the actual sample is introduced. In summary, ELS and DLS measurements on POPC : POPG : DiO 3 : 1 : 0.02 liposomes result in zeta potential $\zeta_p = -30.1 \pm 1.4$ mV and diameter $d = 122.8 \pm 0.6$ nm respectively. Biotinylated liposomes were fabricated POPC : POPG : Biotin PE : DiO 3 : 1 : 0.02 : 0.02 with $\zeta_p = -29.8 \pm 2.9$ mV and $d = 119 \pm 1$ nm. Liposomes used in Fig. S6 are POPC : POPG : DiO 3 : 1 : 0.02 with $\zeta_p = -25.9 \pm 1.2$ mV and $d = 121 \pm 1$ nm.

### Nanofluidic device fabrication

The nanofluidic device is fabricated by injection molding (Engel) of a COC with a $T_g$ of 135 °C (TOPAS 5013) using a nickel shim fabricated from a silicon master (two-step UV lithography and reactive-ion etching processes) as fully described in ref. 18. The injection molded device is sealed by UV-assisted thermal bonding with a 175 μm-thick TOPAS 5013 COC foil. The bonding occurs in two steps at (125 °C) using a lower force and a higher force (0.5–0.7 kN, and 2 kN, 2 minutes per step). The geometry of the device consists of two 5 μm-deep microchannels connected by an array of funnel-shaped nanochannels, with narrow openings of 5 μm on one side and wide openings of 20 μm on the other side. Two different device designs with different length L of the nanochannels were used in this work: in the first design, nanochannels are 295 nm-deep and 440 μm-long. In the second design, nanochannels are 310 nm-deep and 250 μm-long.

### Diffusiophoretic trapping

The device is filled with pure ethanol and washed with 1× PBS. Then, a 1% w/v Pluronic F-127 (Sigma-Aldrich P2443) solution in MilliQ water is introduced for 20 minutes in both microchannels at a pressure drop of 50 mbar maintained by a pressure controller and a 950 mbar pressure drop through the nanochannel (Fluigent MFCS-EX). During the coating, the device is bleached with a green LED at 100% power (TRITC, 4× magnification). To remove the excess Pluronic and establish the salinity gradient, microchannels are washed with a high (10× PBS) and a low ($10^{-3}$ × PBS) salinity solution. First, the microchannels are flushed at 200 mbar pressure drop, and then the salinity solutions are flushed through the nanochannels at 100 mbar pressure drop. Next both microchannels are washed with high and low salinity solutions at 50 mbar pressure drop for 5 minutes and at 5 mbar for 5 minutes to establish the salt gradient in the nanochannels. From this point on, the pressure drops used to drive flows in the microchannels are maintained equal in the low and high salinity microchannels so that there is no pressure driven flow across the nanochannels and the salt gradient is constant. More specifically, the microchannel connected to the narrow side of the nanochannel is filled with a phosphate buffered saline

(PBS) of $C_L$ concentration, and $C_L > C_H$, where $C_H$ is the microchannel solution on the wide side of the nanochannel and the strength of the salinity gradient is characterized as $\ln(C_L/C_H)$. Diffusiophoresis moves the particles towards either higher or lower ionic concentration depending on the physical properties of the system. The concentration of Sodium Chloride (NaCl) is the main contribution to the salinity gradient because of the difference between cation and anion mobilities summarized in the parameter $\beta \simeq -0.2$.[8,9] The diffusivities of the different ionic species used in this work direct the diffusioosmotic fluid flow from the higher toward the lower ionic concentration. Next, liposomes are introduced in the low salinity microchannel ($10^{-3} \times$ PBS) at 50 mbar between the ends of the microchannels. After 1 minute the pressure is brought to zero, and the liposome solution is exchanged from the inlets for a clean $10^{-3} \times$ PBS solution.

### Fluorescence imaging

The DiO signal of the liposomes is imaged using either a 30×/0.5 (Fig. 2a and e) or a 60×/1.4 (Fig. 3a and 4a) objective (Nikon) on an inverted epifluorescence microscope (Nikon Ti2-U) equipped with a sCMOS camera (Photometrics Prime95B, 11 μm pixels) and an LED source at 5% power (CoolLED, pe-300 white SB). Images are recorded using a green emission filter cube (AHF, FITC BrightLine Ex474/Em525/DM495) at 25 frames with 50 ms exposure time. Each field of view of the camera captures the image of several parallel nanochannels. Each nanochannel constitutes a diffusiophoretic trap and a replica experiment. The fluorescence intensity profile used to represent the particle distribution is measured as the fluorescence signal along a nanochannel to which we subtract the mean of the background intensity measured on both sides of the nanochannel of interest. In the osmotic and residual flow calibrations (Fig. S6), the shape of the intensity profile of the dye in the nanochannel is critical and so we first perform a flat field correction of the fluorescence image before measuring the background and signal in each nanochannel.

## Author contributions

RM: conceptualization. PS and CC: experiments and data analysis. PS, CC and RM: writing first draft. All: review and editing.

## Conflicts of interest

The authors declare no conflict of interest.

## Data availability

Data for this article, including timelapse fluorescence imaging corresponding to Fig. 1–4 and S7 is available at https://doi.org/10.11583/DTU.30316021.

Supplementary information (SI): Fig. S1–8 and corresponding experimental procedures. See DOI: https://doi.org/10.1039/d5nr04453g.

## Acknowledgements

## References

1 E. Willms, H. J. Johansson, I. Mäger, Y. Lee, K. E. M. Blomberg, M. Sadik, A. Alaarg, C. I. Smith, J. Lehtiö, S. El Andaloussi, M. J. Wood and P. Vader, Cells release subpopulations of exosomes with distinct molecular and biological properties, *Sci. Rep.*, 2016, **6**, 22519.

2 X. Huang, T. Yuan, M. Tschannen, Z. Sun, H. Jacob, M. Du, M. Liang, R. L. Dittmar, Y. Liu, M. Liang, M. Kohli, S. N. Thibodeau, L. Boardman and L. Wang, Characterization of human plasma-derived exosomal RNAs by deep sequencing, *BMC Genomics*, 2013, **14**, 319.

3 R. P. Carney, R. R. Mizenko, B. T. Bozkurt, N. Lowe, T. Henson, A. Arizzi, A. Wang, C. Tan and S. C. George, Harnessing extracellular vesicle heterogeneity for diagnostic and therapeutic applications, *Nat. Nanotechnol.*, 2025, **20**, 14–25.

4 H. L. Tran, W. Zheng, D. A. Issadore, H. Im, Y.-K. Cho, Y. Zhang, D. Liu, Y. Liu, B. Li, F. Liu, D. T. W. Wong, J. Sun, K. Qian, M. He, M. Wan, Y. Zeng, K. Cheng, T. J. Huang, D. T. Chiu, L. P. Lee, L. Zheng, A. K. Godwin, R. Kalluri, S. A. Soper and T. Y. Hu, Extracellular Vesicles for Clinical Diagnostics: From Bulk Measurements to Single-Vesicle Analysis, *ACS Nano*, 2025, 28021–28109.

5 K. Brennan, K. Martin, S. P. FitzGerald, J. O'Sullivan, Y. Wu, A. Blanco, C. Richardson and M. M. Mc Gee, A comparison of methods for the isolation and separation of extracellular vesicles from protein and lipid particles in human serum, *Sci. Rep.*, 2020, **10**, 1039.

6 C. M. Abreu, B. Costa-Silva, R. L. Reis, S. C. Kundu and D. Caballero, Microfluidic platforms for extracellular vesicle isolation, analysis and therapy in cancer, *Lab Chip*, 2022, **22**, 1093–1125.

7 K. Lee, J. Lee, D. Ha, M. Kim and T. Kim, Low-electric-potential-assisted diffusiophoresis for continuous separation of nanoparticles on a chip, *Lab Chip*, 2020, **20**, 2735–2747.

8 D. C. Prieve, J. L. Anderson, J. P. Ebel and M. E. Lowell, Motion of a particle generated by chemical gradients. Part 2. Electrolytes, *J. Fluid Mech.*, 1984, **148**, 247–269.

9 S. Marbach and L. Bocquet, Osmosis, from molecular insights to large-scale applications, *Chem. Soc. Rev.*, 2019, **48**, 3102–3144.

10 S. Shim, Diffusiophoresis, Diffusioosmosis, and Microfluidics: Surface-Flow-Driven Phenomena in the Presence of Flow, *Chem. Rev.*, 2022, **122**, 6986–7009.

11 N. Shi, R. Nery-Azevedo, A. I. Abdel-Fattah and T. M. Squires, Diffusiophoretic Focusing of Suspended Colloids, *Phys. Rev. Lett.*, 2016, **117**, 258001.

12 S. Shin, O. Shardt, P. B. Warren and H. A. Stone, Membraneless water filtration using CO2, *Nat. Commun.*, 2017, **8**, 15181.

13 N. Singh, G. T. Vladisavljević, F. Nadal, C. Cottin-Bizonne, C. Pirat and G. Bolognesi, Reversible Trapping of Colloids in Microgrooved Channels via Diffusiophoresis under Steady-State Solute Gradients, *Phys. Rev. Lett.*, 2020, **125**, 248002.

14 J. Palacci, B. Abécassis, C. Cottin-Bizonne, C. Ybert and L. Bocquet, Colloidal motility and pattern formation under rectified diffusiophoresis, *Phys. Rev. Lett.*, 2010, **104**, 138302.

15 H. Liu and A. A. Pahlavan, Diffusioosmotic Reversal of Colloidal Focusing Direction in a Microfluidic T-Junction, *Phys. Rev. Lett.*, 2025, **134**, 098201.

16 I. Williams, P. B. Warren, R. P. Sear and J. L. Keddie, Colloidal diffusiophoresis in crossed electrolyte gradients: Experimental demonstration of an "action-at-a-distance" effect predicted by the Nernst-Planck equations, *Phys. Rev. Fluids*, 2024, **9**, 014201.

17 A. Chakra, C. Puijk, G. T. Vladisavljević, C. Cottin-Bizonne, C. Pirat and G. Bolognesi, Surface Chemistry-based Continuous Separation of Colloidal Particles via Diffusiophoresis and Diffusioosmosis, *J. Colloid Interface Sci.*, 2025, **693**, 137577.

18 M. K. Rasmussen, J. N. Pedersen and R. Marie, Size and surface charge characterization of nanoparticles with a salt gradient, *Nat. Commun.*, 2020, **11**, 2337.

19 M. K. Rasmussen, J. N. Pedersen and R. Marie, Label-Free Sensing of Biorecognition on Liposomes, *ACS Sens.*, 2020, **5**, 4057–4063.

20 R. Marie, M. K. Rasmussen and J. N. Pedersen, Quantifying DNA-mediated liposome fusion kinetics with a fluidic trap, *Soft Matter*, 2023, **19**, 2815–2822.

21 M. R. Nejadnik, A. L. Olsson, P. K. Sharma, H. C. Van Der Mei, W. Norde and H. J. Busscher, Adsorption of pluronic F-127 on surfaces with different hydrophobicities probed by quartz crystal microbalance with dissipation, *Langmuir*, 2009, **25**, 6245–6249.

22 Y. Yang, P. G. Rouxhet, D. Chudziak, J. Telegdi and C. C. Dupont-Gillain, Influence of poly(ethylene oxide)-based copolymer on protein adsorption and bacterial adhesion on stainless steel: Modulation by surface hydrophobicity, *Bioelectrochemistry*, 2014, **97**, 127–136.

23 Y. Yang, C. Poleunis, L. Románszki, J. Telegdi and C. C. Dupont-Gillain, Adsorption of a PEO-PPO-PEO triblock copolymer on metal oxide surfaces with a view to reducing protein adsorption and further biofouling, *Biofouling*, 2013, **29**, 1123–1137.

24 J. Jin, F. Huang, Y. Hu, W. Jiang, X. Ji, H. Liang and J. Yin, Immobilizing PEO-PPO-PEO triblock copolymers on hydrophobic surfaces and its effect on protein and platelet: A combined study using QCM-D and DPI, *Colloids Surf., B*, 2014, **123**, 892–899.

25 G. Gyulai, A. Magyar, J. Rohonczy, J. Orosz, M. Yamasaki, S. Bősze and L. P. Kiss, Preparation and characterization of cationic pluronic for surface modification and functionalization of polymeric drug delivery nanoparticles, *eXPRESS Polym. Lett.*, 2016, **10**, 216–226.

26 K. Perez-Toralla, J. Champ, R. Mohamadi, O. Braun, L. Malaquin, J. L. Viovy and S. Descroix, New non-covalent strategies for stable surface treatment of thermoplastic chips, *Lab Chip*, 2013, **13**, 4409–4418.

27 A. Gupta, S. Shim and H. A. Stone, Diffusiophoresis: From dilute to concentrated electrolytes, *Soft Matter*, 2020, **16**, 6975–6984.

28 M. A. Tănase, A. C. Soare, L. M. Dițu, C. L. Nistor, C. I. Mihaescu, I. C. Gifu, C. Petcu and L. O. Cinteza, Influence of the Hydrophobicity of Pluronic Micelles Encapsulating Curcumin on the Membrane Permeability and Enhancement of Photoinduced Antibacterial Activity, *Pharmaceutics*, 2022, **14**, 2137.

29 B. Marta, E. Jakab, M. Potara, T. Simon, F. Imre-Lucaci, L. Barbu-Tudoran, O. Popescu and S. Astilean, Pluronic-coated silver nanoprisms: Synthesis, characterization and their antibacterial activity, *Colloids Surf., A*, 2014, **441**, 77–83.

30 J. Anderson, M. Lowell and D. Prieve, Motion Of A Particle Generated By Chemical Gradients.1. Non-Electrolytes, *J. Fluid Mech.*, 1982, **117**, 107–121.

31 I. Williams, S. Lee, A. Apriceno, R. P. Sear and G. Battaglia, Diffusioosmotic and convective flows induced by a nonelectrolyte concentration gradient, *Proc. Natl. Acad. Sci. U. S. A.*, 2020, **117**, 25263–25271.

32 R. Maier, M. R. Fries, C. Buchholz, F. Zhang and F. Schreiber, Human versus Bovine Serum Albumin: A Subtle Difference in Hydrophobicity Leads to Large Differences in Bulk and Interface Behavior, *Cryst. Growth Des.*, 2021, **21**, 5451–5459.

33 G. Stübiger, M. D. Nairn, T. K. Abban, M. E. Openshaw, L. Mancera, B. Herzig, M. Wuczkowski, D. Senfter and R. M. Mader, MALDI-MS Protein Profiling of Chemoresistance in Extracellular Vesicles of Cancer Cells, *Anal. Chem.*, 2018, **90**, 13178–13182.

34 N. Nezafati, F. Moztarzadeh and S. Hesaraki, Surface reactivity and in vitro biological evaluation of sol gel derived silver/calcium silicophosphate bioactive glass, *Biotechnol. Bioprocess Eng.*, 2012, **17**, 746–754.

35 C. Lee, C. Cottin-Bizonne, A. L. Biance, P. Joseph, L. Bocquet and C. Ybert, Osmotic flow through fully permeable nanochannels, *Phys. Rev. Lett.*, 2014, **112**, 244501.

36 V. Mirshafiee, R. Kim, M. Mahmoudi and M. L. Kraft, The importance of selecting a proper biological milieu for protein corona analysis in vitro: Human plasma versus human serum, *Int. J. Biochem. Cell Biol.*, 2016, **75**, 188–195.

37 R. Rampado, S. Crotti, P. Caliceti, S. Pucciarelli and M. Agostini, Recent Advances in Understanding the Protein Corona of Nanoparticles and in the Formulation of "Stealthy" Nanomaterials, *Front. Bioeng. Biotechnol.*, 2020, **8**, 166.

38 A. Covington and R. Robinson, References Standards For Electrometric Determination, With Ion-Selective Electrodes, Of Potassium And Calcium In Blood Serum, *Anal. Chim. Acta*, 1975, **78**, 219–223.